# Synthesis, Isolation, and Chemical Reactivity Studies of Nanocrystalline Zinc Oxide

Corrie L. Carnes and Kenneth J. Klabunde*

*Department of Chemistry, Kansas State University, Manhattan, Kansas 66506*

*Received November 16, 1999. In Final Form: January 31, 2000*

Nanocrystals of ZnO have been produced by an alkoxide based synthesis involving diethylzinc, *tert*-butyl alcohol, ethanol, and water. The resulting ZnO is in the form of a powder made up of zincite crystallites in the size range of 3−5 nm. These crystallites aggregate together to form larger spherical particles. These spherical particles have been studied by transmission electron microscopy (TEM) and Brunauer−Emmet−Teller (BET) methods and were found to contain many pores and tunnels. It is because of this that an uncharacteristically high surface area is found, averaging about 120 $m^2$/g. As seen with other metal oxides, once they are made as nanoparticles, their reactivity is greatly enhanced. This is thought to be due to morphological differences, whereas larger crystallites have only a small percentage of reactive sites on the surface, smaller crystallites will possess much higher surface concentration of such sites. Elemental analysis, X-ray diffraction, and infrared spectroscopy have been used to characterize this nanoparticle ZnO, and reactions with $CCl_4$, $SO_2$, and paraoxon have demonstrated significantly enhanced reactivity and/or capacity compared with common forms of ZnO powders.

## I. Introduction

Over the past decade many advances have been made in the area of nanoparticles. One of the most important findings was the existence of size-dependent properties. Changing the materials particle/crystal size can actually alter properties, which were formally thought to be constant for a given material. Gold particles were found to have a melting point that was dependent on the particle size.[1] Magnetic materials were found to have coercive forces that could be manipulated by changing the particle size.[2−6] In semiconductors band gaps were found to be particle size dependent.[7−11] Unique surface chemistry was also attributed to nanoparticles due to the discovery that chemical reactivity is increased as a particle is made smaller.[12−15]

ZnO nanoparticles have been extensively studied over the past years because of their size-dependent electronic and optical properties as a semiconductor. Many preparation methods have been studied and used extensively. Reactions involving diethylzinc with alcohols have also been investigated. In 1965 Coates and Ridley published a reaction between diethylzinc and an alcohol to form alkylzinc alkoxides.[16] This however was never carried further to produce an oxide. In 1993 Na, Walters, and Vannice published data on high surface area ZnO by allowing ammonium carbonate to react with zinc nitrate hydrate.[17] The ZnO produced by this method was found to have a surface area up to 30 $m^2$/g. In 1996 Heistand and Chia reported reactions between diethylzinc and *tert*-butyl alcohol to form an alkylzinc alkoxide.[18] This alkylzinc alkoxide was then allowed to react with toluene, ethanol, and water to form ZnO. This ZnO was characterized by having surface areas of 6−70 $m^2$/g, and a crystallite size of 6−15 nm. More recently, Meulenkamp was able to form ZnO nanoparticles by allowing the reaction of zinc acetate solutions with LiOH.[19] The ZnO produced by this method was found to have a size range of 2−7 nm, and isolation of significant amounts of pure material was not reported.

Attempts to characterize the optical properties of ZnO nanoparticles have been made by many research groups.[20−22] One of the important advances was the observation of new continua in addition to the well-known ZnO band gap. Interesting research has also been conducted to characterize the electronic properties of nanoparticle ZnO.[23−24]

(1) Buffat, P.; Borel, J. P. *Phys. Rev. A* **1976**, *13*, 2287−2298.
(2) Gangopadhyay, S.; Hadjipanyis, G. C.; Dale, B.; Sorenson, C. M.; Klabunde, K. J.; Papaefthymiou, V.; Kosikas, A. *Phys. Rev. B* **1992**, *45*, 9778−9787.
(3) Klabunde, K. J.; Zhang, D.; Glavee, G. N.; Sorenson, C. M.; Hadjipanyis, G. C. *Chem. Mater.* **1994**, *6*, 784−787.
(4) Cullity, B. D. *Introduction to Magnetic Materials*; Addison-Wesley: 1972.
(5) Easom, K. A.; Klabunde, K. J.; Sorenson, C. M.; Hadjipanyis, G. C. *Polyhedron* **1994**, *13*, 1197−1223.
(6) Meikelijohn, W. H.; Bean, C. P. *Phys. Rev.* **1957**, *105*, 904−913.
(7) Steigerwald, M. L.; Brus, L. E. *Acc. Chem. Res.* **1990**, *23*, 183−188.
(8) Wang. Y.; Herron, N. *Phys. Rev. B* **1990**, *42*, 7253−7255.
(9) Johansson, K. R.; McLendon, G.; Marchetti, A. P. *Chem. Phys. Lett.* **1991**, *179*, 321−324.
(10) Rosetti, R.; Hull, R.; Gibson, J. M.; Brus, L. E. *J. Chem. Phys.* **1985**, *83*, 1406−1410.
(11) Dannhauser, T.; O'Neil, M.; Johansson, K. R.; Whitten, D.; McLendon, G. *J. Phys. Chem.* **1953**, *57*, 670−673.
(12) Koper, O.; Li, Y. X.; Klabunde, K. J. *Chem. Mater.* **1993**, *5*, 500−505.
(13) (a) Stark, J. V.; Park, D. G.; Lagadic, I.; Klabunde, K. J. *Chem. Mater.* **1996**, *8*, 1904−1912. (b) Klabunde, K. J.; Stark, J.; Koper, O.; Mohs, C.; Park, D. G.; Decker, S.; Jiang, Y.; Lagadic, I.; Zhang, D. *J. Phys. Chem.* **1996**, vol. 100, No. 30, 12142.
(14) Stark, J. V.; Klabunde, K. J. *Chem. Mater.* **1996**, *8*, 1913−1918.
(15) Itoh, H.; Utampanya, S.; Stark, J. V.; Klabunde, K. J.; Schlup, J. R. *Chem. Mater.* **1993**, *5*, 71−77.
(16) Coates, G. E.; Ridley, D. *J. Chem. Soc.* **1965**, 1870.
(17) Na, B.; Walters, A.; Vannice, M. *J. Catal.* **1993**, *140*, 585.
(18) Heistand, R.; Chia, Y. *Mater. Res. Soc. Symp. Proc.* **1986**, vol. *73*, 93.
(19) Meulenkamp, E. A. *Phys. Chem. B* **1998**, *102*, 5566−5572.
(20) Monticone, S.; Tufeu, R.; Kanaev, A. V. *J. Phys. Chem. B* **1998**, *102*, 2854−2862.
(21) Bahnemann, D. W.; Kormann, C.; Hoffmann, M. R. *J. Phys. Chem.* **1987**, *91*, 3789−3798.
(22) Nyffenegger, R. M.; Craft, B.; Shaaban, M.; Gorer, S.; Erley, G.; Penner, R. M. *Chem. Mater.* **1998**, *10*, 1120−1129.
(23) Rensmo, H.; Keis, K.; Lindstrom, H.; Sodergren, S.; Solbrand, A.; Hagfeldt, A.; Lindquist, S. E.; Wang, L. N.; Muhammed, M. *J. Phys. Chem. B* **1997**, *101*, 2598−2601.

10.1021/la991498p CCC: $19.00 
Published on Web 03/11/2000

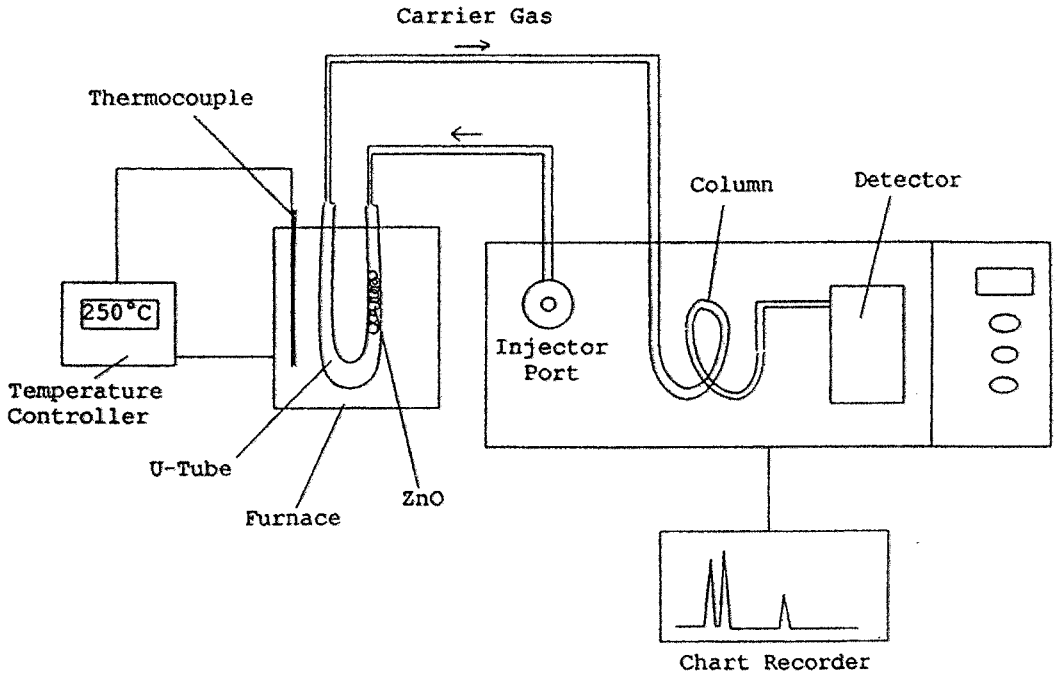


**Figure 1.** Schematic of the GC setup.

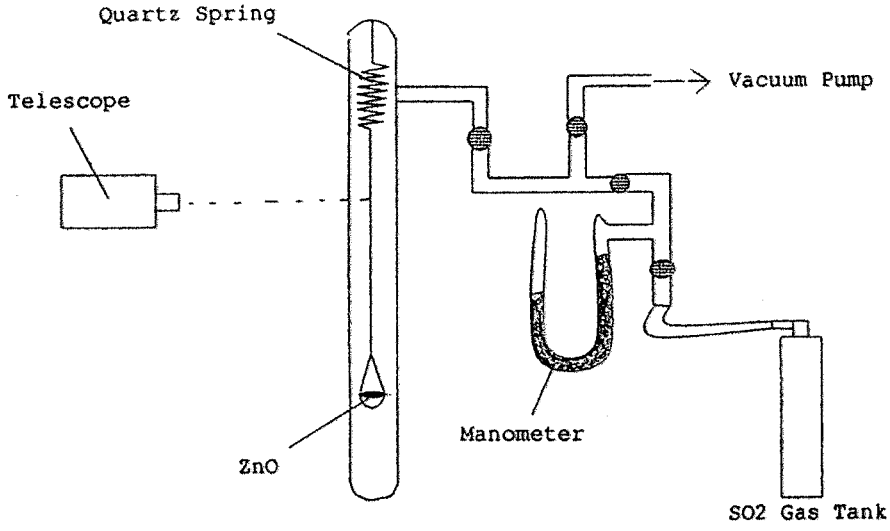


**Figure 2.** Schematic of the spring balance setup.

This paper describes, first, the synthesis and isolation of multigram amounts of pure nanocrystalline ZnO powder and, second, the unique chemical properties of this material. The synthesis involves allowing diethylzinc to react with *tert*-butyl alcohol in the presence of hexanes. Then this solution is allowed to react with a mixture of water and ethanol, and a colloidal dispersion is formed. Upon solvent removal, a fine powder was obtained, which was then heat treated under argon flow. The powder is characterized by 110−140 $m^2/g$ surface area, 2−5 nm crystallite size, and an unprecedented high reactivity. A unique feature of this approach is the intermediate Zn-(O-*t*-Bu)$_2$ species that allows a high quality sol to be formed upon hydrolysis, which leads to very high surface areas and small crystallite size. In addition, our method yields relatively large amounts of pure, nanocrystalline powder.

(24) Redmond, G.; O'Keeffe, A.; Burgess, C.; MacHale, C.; Fitzmaurice, D. *J. Phys. Chem.* **1993**, *97*, 11081−11086.

## II. Experimental Section

**A. Preparation of Alkoxide Based, Nanocrystalline (NC) ZnO.** The reactions involved in the preparation are shown.

$$Zn(CH_2CH_3)_2 + 2(CH_3)_3COH \rightarrow Zn[OC(CH_3)_3]_2 + 2CH_3{-}CH_3$$

$$Zn[OC(CH_3)_3]_2 + 2H_2O \rightarrow Zn(OH)_2 + 2(CH_3)_3COH$$

$$Zn(OH)_2 \rightarrow ZnO + H_2O$$

The preparation consists of three main steps:

1. Synthesis of the zinc oxide powder. The chemicals used in the synthesis were directly from the company without further purification. In a glovebox 40 mL (0.040 mol) of 1.0 M diethylzinc in hexanes (Aldrich) was added to a 500 mL round-bottom flask. This was removed from the glovebox and placed under a head of argon gas, placed on a stir plate and cooled to 0 °C with an ice bath.

A solution of 5.8 g (0.080 mol) of *tert*-butyl alcohol (Fisher) in 60 mL of hexanes (Fisher) was added to the cooled diethylzinc

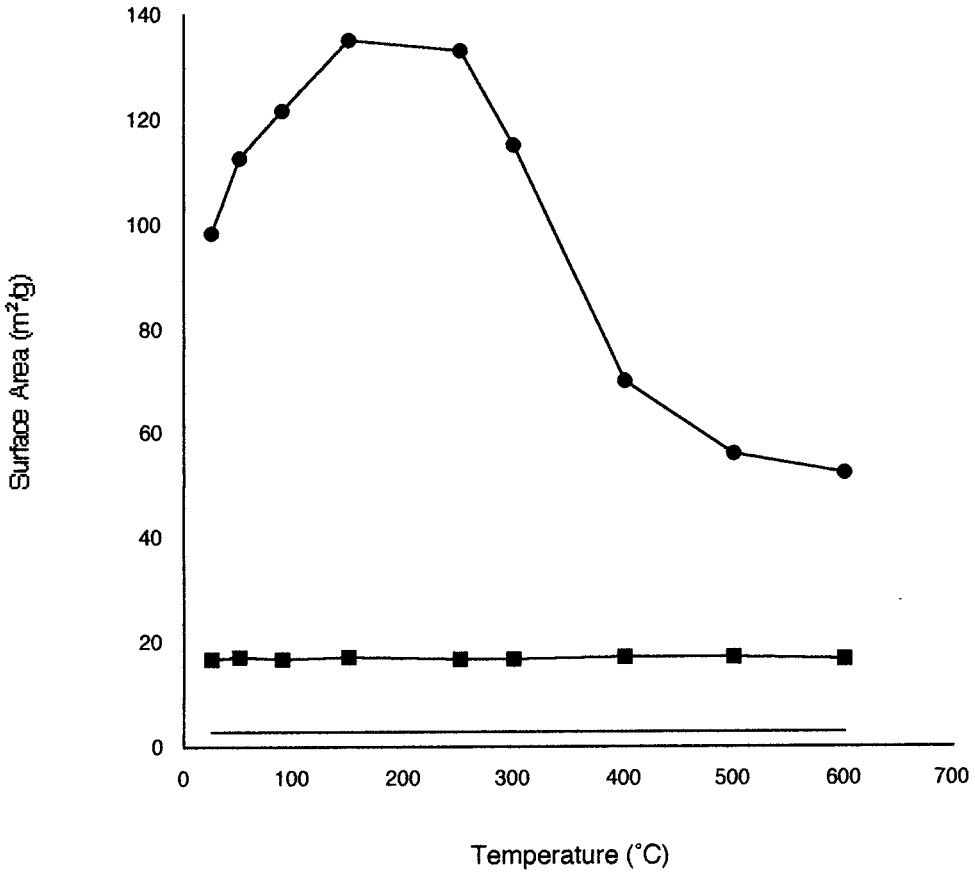


**Figure 3.** Surface area vs temperature: (no symbol) CM−ZnO-1, (squares) CM−ZnO-2, and (circles) NC−ZnO.

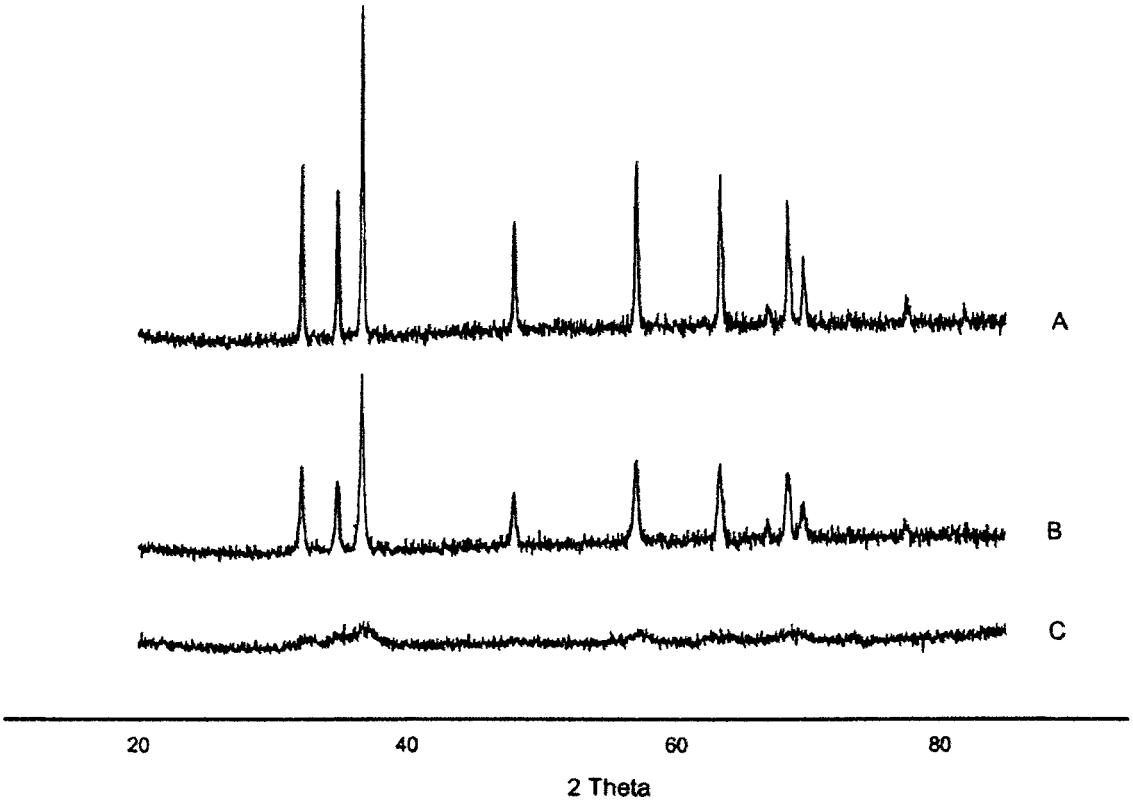


**Figure 4.** X-ray diffraction patterns: (A) CM−ZnO-1, (B) CM−ZnO-2, and (C) NC−ZnO.

solution via syringe. This solution was added over a time span so that the release of ethane was not extremely violent. Once the solution was completely added, the ice bath was removed and the reaction was allowed to come to room temperature (about 25 °C). The reaction was then stirred at room temperature for 2 h. During this time the reaction mixture remained a clear colorless solution.

A solution of 1.44 mL (0.080 mol) of water in 140 mL of absolute

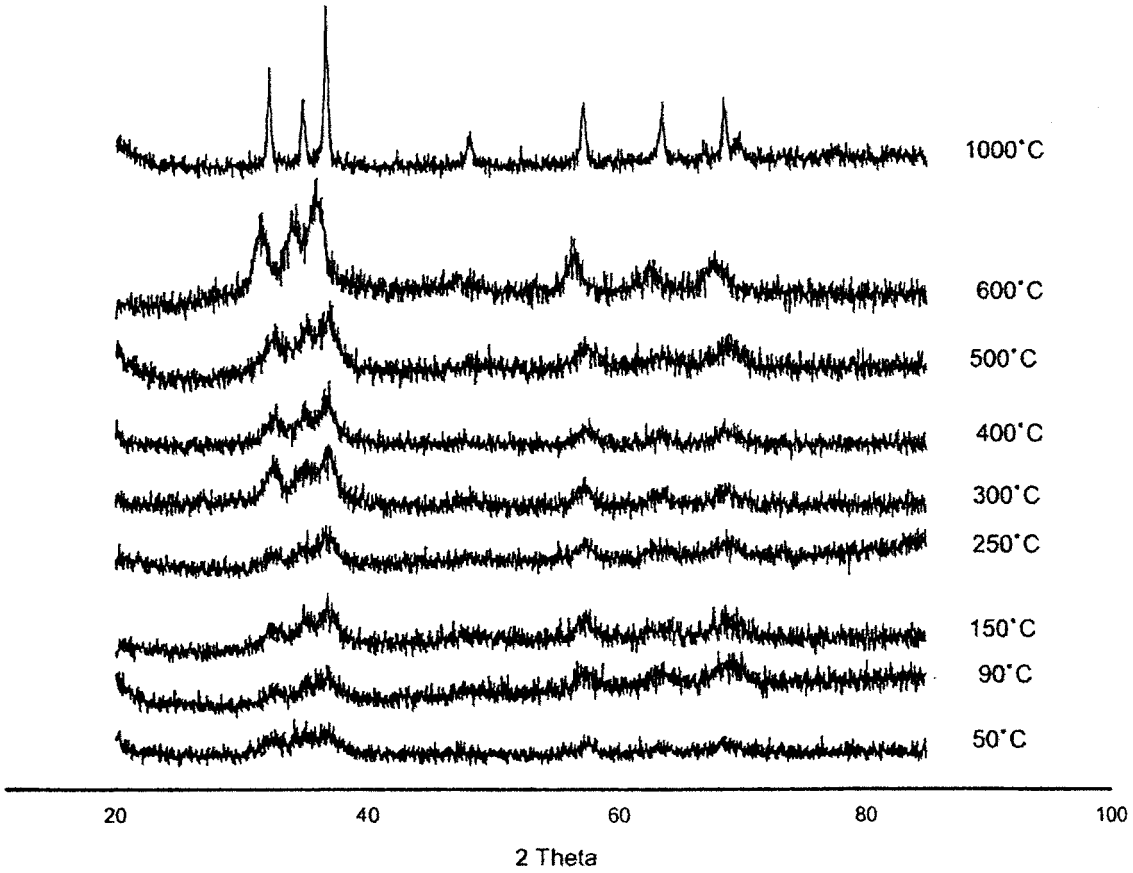


**Figure 5.** X-ray diffraction patterns of NC−ZnO after heat treating at 50, 90, 150, 250, 300, 400, 500, 600, and 1000 °C.

ethanol (McCormick) was then added to the reaction mixture. Once the solution was completely added, the reaction was allowed to stir for an additional 2 h. The zinc oxide slowly formed a white colloidal solution.

2. Isolation of the zinc oxide powder. After the reaction was complete, the argon line was removed and the reaction mixture was poured into a Schlenk tube. This was then connected to a vacuum line attached to a second liquid nitrogen trap. While the reaction was being stirred at 25 °C, all of the solvent was condensed from the Schlenk tube to the second trap. This left a dry, white zinc oxide powder with a yield of 2.9 g (90% yield).

3. Activation heat treatment of the zinc oxide powder. The dry powder was then placed in another Schlenk tube. This was connected to a flow of argon and surrounded by a furnace. The furnace was connected to a temperature controller, and the temperature was slowly raised from room temperature to 90 °C where it was heated for 15 min. Next the temperature was slowly raised from 90 to 250 °C where it was heated for an additional 15 min. After the heat treatment was complete the furnace was turned of and allowed to cool to room temperature. The zinc oxide powder remained white. Heat treatment was conducted under dynamic vacuum and compared to the argon flow method, and both methods were found comparable.

Commercial samples of the highest surface area ZnO available were purchased from Fisher (CM−ZnO-1) and Nanophase Materials (CM−ZnO-2).

**B. Characterization of NC−ZnO.** Transmission electron microscopy (TEM) studies were carried out by adding dry ethanol to the heat-treated ZnO, and sonicating this slurry. A drop of this slurry was then placed onto a carbon coated copper grid. TEM experiments were performed by Dan Boyle at the KSU Microscopy and Image Processing Facility using a Philips 201 TEM.

Surface area measurements were done by the Brunauer−Emmet−Teller (BET) method using both Micromeritics Flowsorb II 2300 and Quantachrome NOVA 1200 instrumentation; 150 mg samples under an argon flow were heated to the desired temperature. The samples were allowed to cool to room temperature and then further cooled to 77 K where the nitrogen adsorption measurements were measured at different pressures.

Powder X-ray diffraction (XRD) studies were carried out using a Scintag XDS 2000 spectrometer. Cu Kα radiation was the light source used with applied voltage of 40 kV and current of 40 mA. The $2\theta$ angles ranged from 20 to 85° with a speed of 2°/min.

Fourier transform infrared spectroscopy (FTIR) techniques were carried out on an RS-1 FTIR spectrometer from Mattson with a liquid nitrogen cooled MCT detector. Heat-treated samples of both NC−ZnO and CM−ZnO were made into KBr pellets and studied.

Elemental analysis of NC−ZnO was conducted by Galbraith Laboratories.

**C. Reaction of ZnO with $CCl_4$.**

$$2ZnO + CCl_4 \rightarrow CO_2 + 2ZnCl_2$$

The reaction between ZnO and $CCl_4$ was carried out to characterize the chemical reactivity of the ZnO. These reactions were conducted in a U-tube that was connected to a gas chromatograph (GOW-MAC gas chromatograph series 580), see Figure 1.[25] The U-tube was made of Pyrex and connected between the injector port and the column (Alltech Chromosorb W-HP). A ZnO sample (0.100 g) was placed in the U-tube between two small plugs of quartz wool. The most favorable temperature for the reaction was found to be 250 °C, so the U-tube was heated at 250 °C. The injector port was kept at 100 °C. Injections of 2 $\mu$L of $CCl_4$ were made every 7 min. Any $CO_2$ coming off the sample, or $CCl_4$ that was not destroyed, was then sent via helium (20 $cm^3$/min) through the column (90 °C) to be separated. They were then detected by

(25) Koper, O. B.; Lagadic, I.; Volodin, A.; Klabunde, K. J. *Chem. Mater.* **1997**, *9*, 2468.

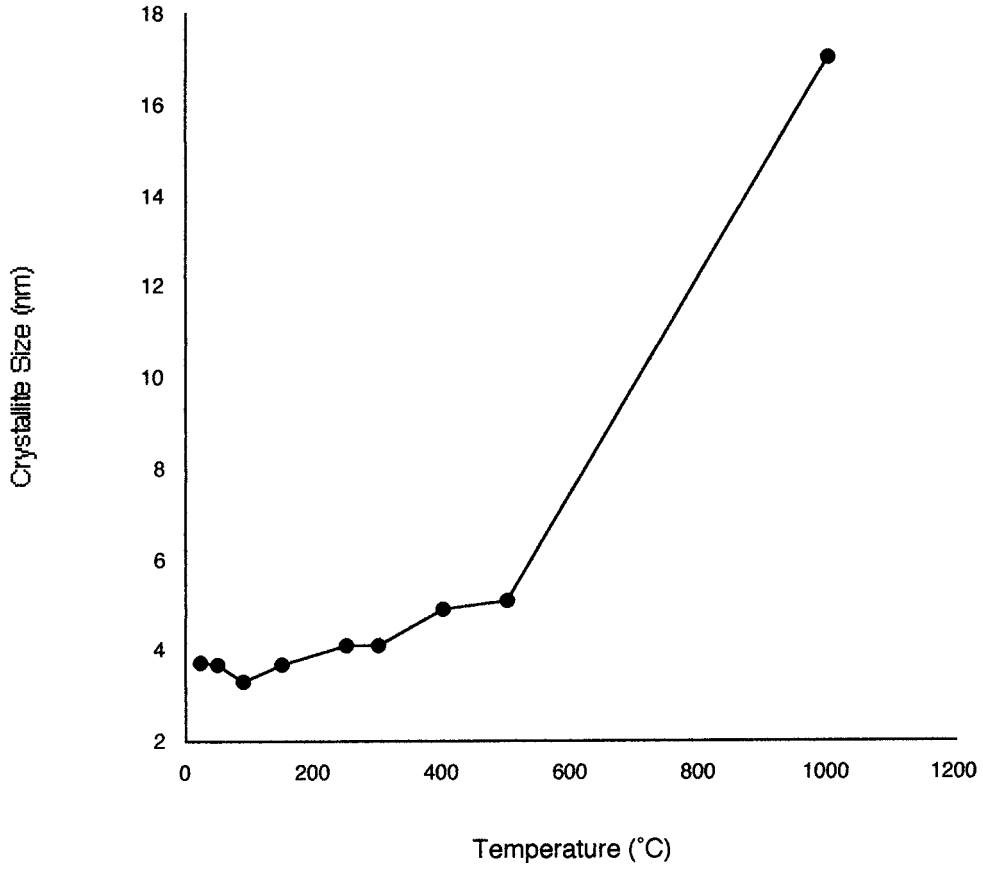


**Figure 6.** Crystallite size vs temperature of NC−ZnO.

a thermal conductivity detector (120 °C) and peak areas recorded. Injections of $CCl_4$ were made until the ZnO bed had been exhausted.

**D. Sulfur Dioxide Adsorption on Zinc Oxide.** A quartz spring balance was used to measure the adsorption of $SO_2$ onto ZnO. The apparatus consists of a basket, which is used to hold the sample; this is attached to a quartz spring.[13] The basket and the spring are closed within the vacuum line. The $SO_2$ gas tank is also attached to the vacuum line. The schematic of the spring balance is shown in Figure 2. As the $SO_2$ adsorbs onto the ZnO in the basket, the weight change causes the spring to move, and this movement is noted by the telescope. Once the telescope is calibrated it is accurate to ±0.1 mg.

Because of the electrostatic properties of the ZnO powder, it was found to be much easier and more accurate to work with ZnO granules. Using ZnO granules helped to eliminate losses during transfers, weighing, and dynamic vacuum. Therefore, the samples were first pressed into pellets at 1000 lbs load and then crushed and sifted through a mesh to achieve granules of uniform size of 0.250−1.17 mm. By using a relatively low pelletization pressure, only a small change in surface area resulted.

Granules (100 mg) of ZnO were placed into the basket on the spring balance. The samples were placed under dynamic vacuum for 1 h at room temperature. After evacuation, the vacuum line was closed to the pump and the spring position was noted. The $SO_2$ gas was allowed to fill the vacuum line, including the spring balance to the desired pressure. The spring position was noted over the next hour. This was followed by 100 min of evacuation to remove all physisorbed species. After the evacuation, the spring position was noted again indicating the presence of remaining strongly chemisorbed species.

**E. Destructive Adsorption of Diethyl 4-Nitrophenyl Phosphate.** The destructive adsorption of diethyl 4-nitrophenyl phosphate (DNPP, also called paraoxon) was carried out of to determine the capacity of the ZnO to dissociatively chemisorb a polar organophosphorus compound that is considered a chemical warfare mimic. A 0.100 g ZnO sample was placed into a 250 mL round-bottom flask that had been flushed with argon, 100 mL of dry pentane was then added to the flask, and stirring commenced. Then 8 $\mu$L of paraoxon was added to the flask, and ultraviolet/visible spectroscopy (SIM Aminco Milton Roy 3000 array) was used to monitor the disappearance of paraoxon at 270 nm wavelength, by extracting samples at desired intervals. This reaction was monitored every 20 min for 3 h and then at 20 h. The powder was then filtered and FTIR was then used to detect adsorbed species on the solid. The used solid was also washed with 10 mL portions of $CH_2Cl_2$; IR spectra of the extracted $CH_2Cl_2$ show that no adsorbed species were removed.

## III. Results and Discussion

**A. Morphology.** By careful characterization of the ZnO samples, it became clear that the NC−ZnO samples had morphology different from that of the commercial (CM) ZnO samples. This is most likely caused by the low temperature "soft chemical" preparation method. Commercial ZnO is most commonly prepared by high temperature methods, and CM−ZnO-1 typically had surface areas within the range of 2−4 $m^2/g$, and CM−ZnO-2 had surface areas of 16−20 $m^2/g$. Our NC−ZnO samples typically possessed surface areas within the range of 110−130 $m^2/g$ after heat treatment at 250 °C. When heated at higher temperatures, the crystallites began to sinter, and as a result, the surface areas decreased. Figure 3 shows the heat treatment temperature dependence we observed. Using BET, it was also possible to obtain data on the pore structures. The average NC−ZnO sample after heat treatment possessed pores that were about 11 nm in diameter and were open at both ends.

(26) Azároff, L. V. *The Powder Method in X-ray crystallography*; McGraw-Hill Book Co.: New York, 1958; Chapter 16.

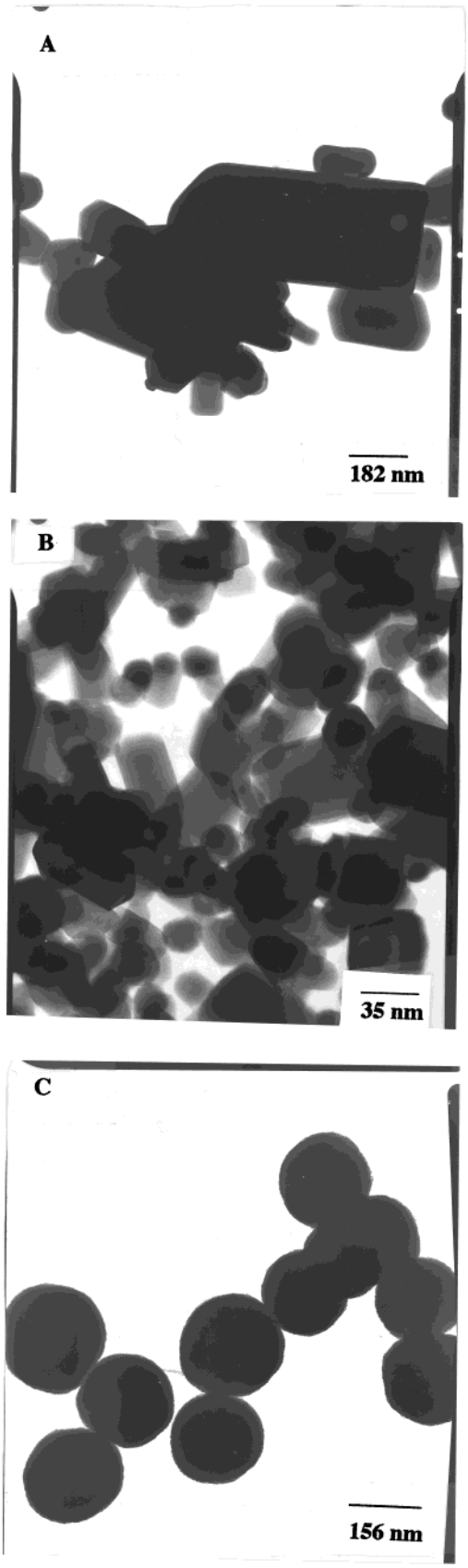


**Figure 7.** Transmission electronmicroscope images of (A) CM−ZnO-1, (B) CM−ZnO-2, and (C) NC−ZnO.

From XRD we obtained diffraction patterns that showed the NC−ZnO sample to be less crystalline than the commercial ZnO samples. The NC−ZnO had much broader and less intense peaks; see Figure 4. This is due to particle size broadening, which occurs when a sample is made up of very small crystallites, and the broadness of the peaks can be used to calculate crystallite size using the Scherrer equation.[26]

From the diffraction patterns crystallite size of NC−ZnO was determined as the temperature was increased. The results show that the NC−ZnO has a significantly smaller crystallite size than the commercial ZnO samples; indeed, the average crystallite size for NC−ZnO activated at 250 °C was found to be 2−5 nm, whereas the average crystallite size for CM−ZnO-1 was 41−45 nm, and CM−ZnO-2 was 32−35 nm. These data confirmed that as temperature increased, the crystallites grew. Figure 5 shows the X-ray diffraction patterns of NC−ZnO heated from 50 to 1000 °C. Figure 6 shows the crystallite size as plotted vs temperature.

TEM was also used to evaluate the NC−ZnO and CM−ZnO samples. Figure 7 shows TEM photographs, and both of the CM−ZnO samples consist of single crystals having an estimated crystallite size of 76 nm (CM−ZnO-1) and 42 nm (CM−ZnO-2). The NC−ZnO sample, however, consists of rather large spherical agglomerations of crystallites having an average overall particle size of 260 nm. By compiling data from XRD, TEM, and BET, we have concluded that the NC−ZnO samples are made up of 3−5 nm crystallites which loosely agglomerate into larger, very porous spherical particles. High-resolution TEM may yield additional information about the individual crystallites and will be investigated soon.

**Table 1. Reaction of Pulses of $CCl_4$ with ZnO Samples at 250 °C**

| sample | breakthrough | saturation | molar ratio |
|---|---|---|---|
| NC−ZnO | 6 | 58 | 1 mol $CCl_4$:3.4 mol ZnO |
| CM−ZnO-1 | 1 | 2 | 1 mol $CCl_4$:1690 mol ZnO |
| CM−ZnO-2 | 1 | 4 | 1 mol $CCl_4$:92 mol ZnO |

**Table 2. Adsorption of $SO_2$ on ZnO Samples at Room Temperature**

| sample | total molecules $SO_2/nm^2$ adsorbed | molecules $SO_2/nm^2$ physisorbed | molecules $SO_2/nm^2$ chemisorbed |
|---|---|---|---|
| NC−ZnO | 10 | 2.2 | 7.8 |
| CM−ZnO-1 | 0 | 0 | 0 |
| CM−ZnO-2 | 8.2 | 8.2 | 0 |

**Table 3. Destructive Adsorption of Paraoxon in Pentane on ZnO Powders**

| sample | molar ratio |
|---|---|
| NC−ZnO | 1 mol paraoxon:47 mol ZnO |
| CM−ZnO-1 | 1 mol paraoxon:1100 mol ZnO |
| CM−ZnO-2 | 1 mol paraoxon:360 mol ZnO |

**Table 4. FTIR Bands for Free Paraoxon, and Adsorbed Paraoxon**

| free paraoxon | assignment | adsorbed paraoxon | assignment |
|---|---|---|---|
| 860 | $\nu$(C−N) | 860 | $\nu$(C−N) |
| 930 | $CH_3$ rock | 930 | $CH_3$ rock |
| 1045 | $\nu$(Et−O−(P)) | 1045 | $\nu$(C−O−(P)) |
| 1107 | $CH_3$ rock | 1107 | $CH_3$ rock |
| 1164 | $CH_3$ rock | 1160 | $CH_3$ rock |
| 1232 | $\nu$(P−O−(Ar)) | | |
| 1296 | $\nu$(P═O) | 1213, 1253 | $\nu$(P═O) |
| 1348 | $\nu_s$(N−O) | 1313 | $\nu_s$(N−O) |
| 1491 | $\nu$(C−C ring) | 1491 | $\nu$(C−C ring) |
| 1526 | $\nu_{as}$(N−O) | | |
| 1593 | $\nu$(C−C ring) | 1593 | $\nu$(C−C ring) |

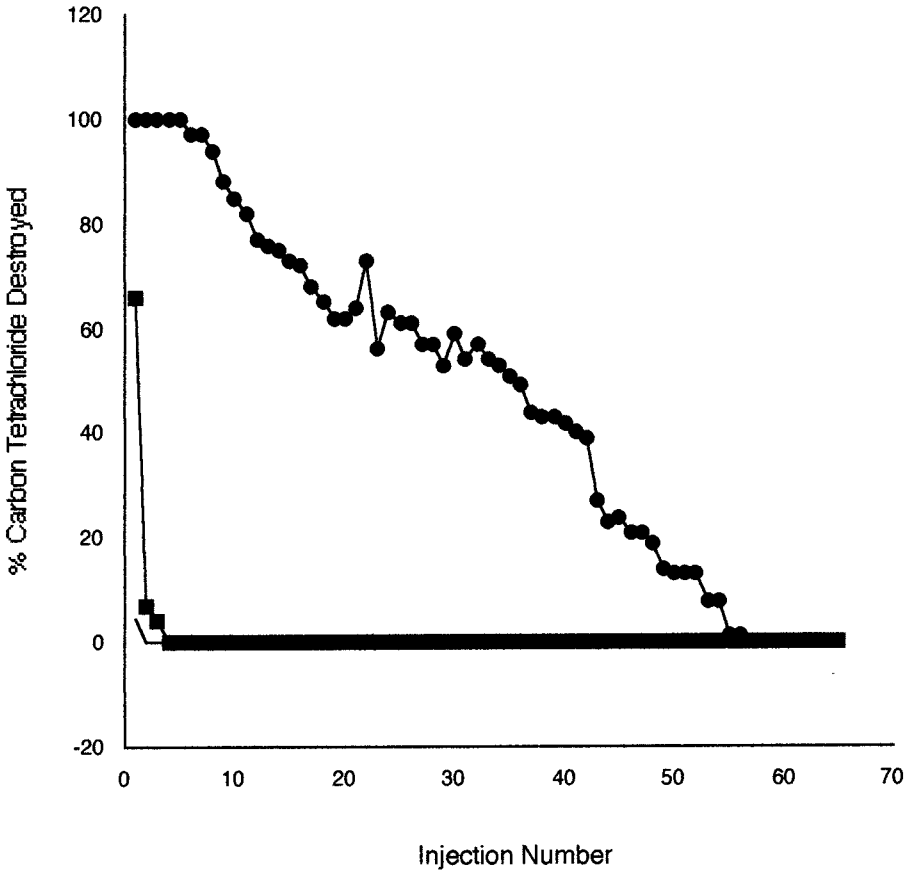


**Figure 8.** % $CCl_4$ destroyed vs injection number: (no symbols) CM−ZnO-1, (squares) CM−ZnO-2, and (circles) NC−ZnO.

Elemental analysis of NC−ZnO preheat-treated to 250 °C under argon flow showed 79% Zn (calculated 80%) and <0.50% carbon and <0.50% hydrogen. These results indicate the presence of some residual $OH/H_2O$ as well as adsorbed $CO_2$ which are indicated by IR; see Figure 8. There do not appear to be any residual OR groups, although some of this carbon maybe present in the form of amorphous graphite. If $CO_2$ and surface OH are assumed to be the only adsorbed species, a formula $ZnO(OH)_{0.004}$-$(CO_2)_{0.03}$ fits the data (oxygen by difference).

**B. Unique Chemical Reactivities. 1. Reaction of ZnO with $CCl_4$.** The reaction of $CCl_4$ and ZnO was carried out to understand the destructive adsorption abilities of ZnO, toward a model chlorocarbon at elevated adsorption temperatures.

$$2ZnO + CCl_4 \rightarrow CO_2 + 2ZnCl_2$$

These reactions were conducted via the pulse method and the products were identified by GC; see Figure 1.[25] The breakthrough injection, saturation injection, and molar ratios are reported in Table 1. The breakthrough injection of the reaction is the first injection that there is not a complete destruction of $CCl_4$, and it is sensed at the detector. The saturation injection is the first injection that 100% of the injected $CCl_4$ is seen at the detector. Figure 8 shows a graph of the % $CCl_4$ destroyed vs the injection number. For comparison the CM−ZnO-1 sample showed breakthrough at the first injection and was saturated by the second injection. The CM−ZnO-2 samples also showed breakthrough on the first injection and were saturated on the fourth injection. The NC−ZnO samples had much higher breakthrough numbers, destroying 100% of the injected $CCl_4$ for the first four to five injections. The NC−ZnO samples gave partial reactions until the 56th−58th injection where saturation occurred. The theoretical molar ratio of ZnO:$CCl_4$ is 2:1. The experimental results showed that the NC−ZnO samples were much more reactive than the CM−ZnO. The experimental molar ratios for NC−ZnO samples were 3.4:1 and 3.7:1, whereas the experimental molar ratios for CM−ZnO were much higher (Table 1 and Figure 8).

**2. Sulfur Dioxide Adsorption on Zinc Oxide.** Adsorption of $SO_2$ was carried out to learn if the adsorption properties are different for nanocrystals, when compared to commercial microcrystals. These reactions were carried out on the quartz spring balance; see Figure 2. The amount of $SO_2$ required for a monolayer of gas can be calculated. Using 19.2 $Å^2$ as the area of an $SO_2$ molecule, it can be determined that 5.2 molecules of $SO_2/nm^2$ would form a monolayer. The experimental results showed that at atmospheric pressure and room temperature, $SO_2$ adsorbed onto NC−ZnO up to 11 molecules of $SO_2/nm^2$, whereas on CM−ZnO-2 there were 8.2 molecules of $SO_2/nm^2$ adsorbed, and on CM−ZnO-1 there was not any adsorption observed (Table 2). These data indicate that NC−ZnO, and CM−ZnO-2 efficiently adsorb $SO_2$ in multilayers. After adsorption had ceased the samples were subjected to dynamic vacuum for 100 min to remove the physisorbed species. After this vacuum treatment, there remained 8.4, and 7.9 molecules of $SO_2/nm^2$ present chemisorbed onto the two NC−ZnO samples studied. This vacuum treatment removed all of the adsorbed SO2 from the CM−ZnO-2 sample. These results indicate that the NC−ZnO samples have a high capacity for chemisorption

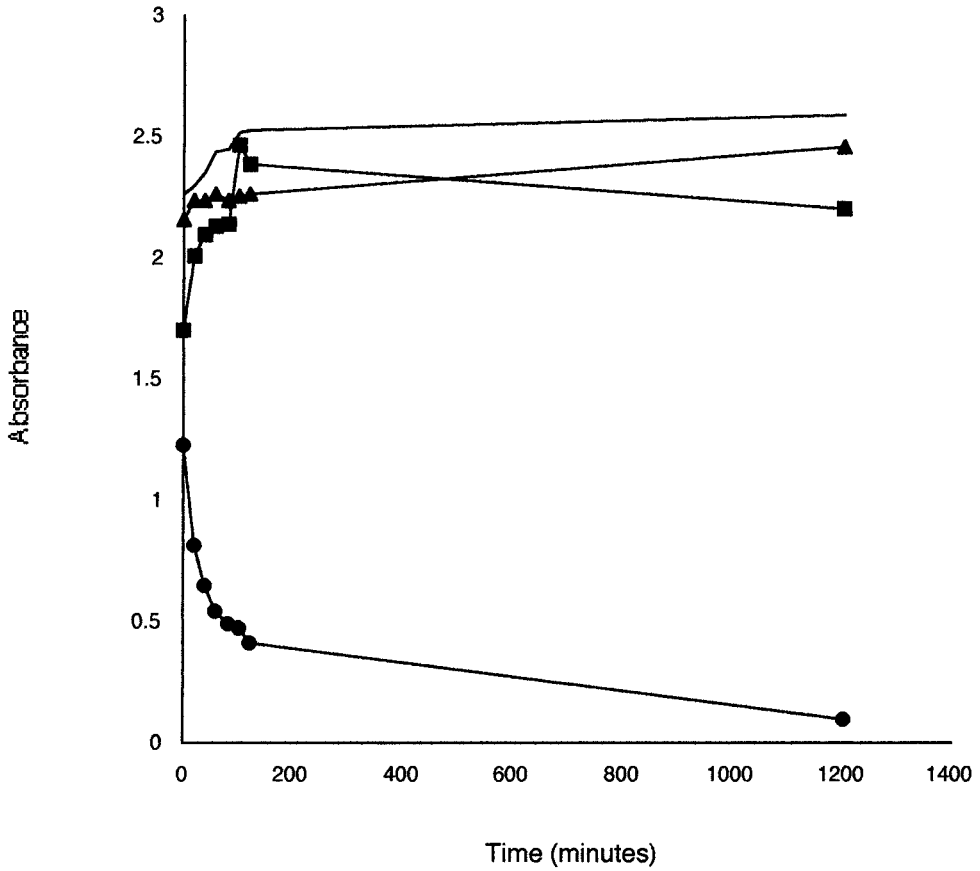


**Figure 9.** Disappearance of a paraoxon absorbance band vs time: (no symbol) blank, (triangles) CM−ZnO-1, (squares) CM−ZnO-2, and (circles) NC−ZnO.

of $SO_2$ (Table 2) per unit surface area, indicating an intrinsically higher activity.

**3. Destructive Adsorption of Diethyl 4-Nitrophenyl Phosphate (Paraoxon).** The adsorption of paraoxon was carried out to compare the rates and capacities for the ZnO sample to dissociatively chemisorb a polar organic, more specifically an insecticide and a warfare mimic. By monitoring the disappearance of an UV band for paraoxon in pentane the data shown in Table 3 and Figure 9 were obtained, and the results are striking. Neither CM−ZnO sample adsorbed much paraoxon, while NC−ZnO rapidly adsorbed the entire sample and developed a bright yellow color, indicating the likely formation of the *p*-nitrophenoxide anion on the surface.

Additional experiments with larger and larger amounts of paraoxon indicated that about 5.5 $\mu$L of liquid paraoxon ($2.55 \times 10^{-5}$ mol, $1.53 \times 10^{19}$ molecules) was taken up by 0.100 g of NC−ZnO. One molecule of paraoxon dissociated and with the *p*-nitrophenoxide lying flat would occupy about 1 $nm^2$ of surface area. In a 0.100 g sample $12.0 \times 10^{18}$ $nm^2$ surface is available, and so we can estimate that about 1.3 monolayers are adsorbed under these conditions (room temperature, 0.01 M concentration in pentane).

After the reaction was complete the powders were filtered, and IR studies were done on the solids. The results from the IR show that the NC−ZnO samples have many new species adsorbed to the powder, whereas the commercial ZnO samples have little if any new species adsorbed. Table 4 gives IR spectra assignments for free paraoxon and for paraoxon adsorbed on ZnO which are based on literature.[27−29] Figure 10 shows the IR spectra taken following the reaction with paraoxon: (A) CM−ZnO-1, (B) CM−ZnO-2, and (C) NC−ZnO. It appears that several things change in the FTIR when paraoxon is adsorbed on ZnO. A band at 1526 $cm^{-1}$ assigned to $\nu_{as}$(N−O) in $ArNO_2$ disappears; the band $\nu$(P═O) at about 1296 $cm^{-1}$ is broadened and shifted to approximately 1240 $cm^{-1}$ (two peaks at 1213 and 1253 $cm^{-1}$). Also, the original peak for free paraoxon at 1232 $cm^{-1}$ assigned to $\nu$(P−O−Ar stretch has either disappeared (there is no new peak present at the expected lower wavelength), or it is weakened and enveloped in the new $\nu$(P═O) band in the 1213−1253 $cm^{-1}$ range. The band due to $\nu$(P−O−Et) at 1045 $cm^{-1}$ does not change much (see Table 4), suggesting that the EtO−P moieties are not perturbed or destroyed. We tentatively conclude from these data that the P═O bond is strongly perturbed through binding to Lewis acid sites on the ZnO surface and that the P−OAr bond is probably broken.

## Conclusion

Wurtzite phase ZnO nanocrystals have been synthesized using a modified sol−gel procedure. Using this procedure we obtain the following characteristics: (1) the ZnO nanoparticles have a crystallite size of 3−5 nm; (2) the average NC−ZnO surface area is 120 $m^2/g$; (3) the small ZnO crystallites agglomerate into larger spherical particles

(27) Li, Y.; Schlup, J.; Klabunde, K. J. *Langmuir* **1991**, *7*, 1388.

(28) Lin-Vien, D.; Colthup, N.; Fateley, W.; Grasselli, J. *The Handbook of Infrared and Raman Characteristic Frequencies of Organic Molecules*; Academic: New York, 1991.

(29) Pretsch, E.; Clerc, T.; Seibl, J.; Simon, W. *Tables of Spectral Data for Structure Determination of Organic Compounds*; Springer-Verlag: New York, 1989.

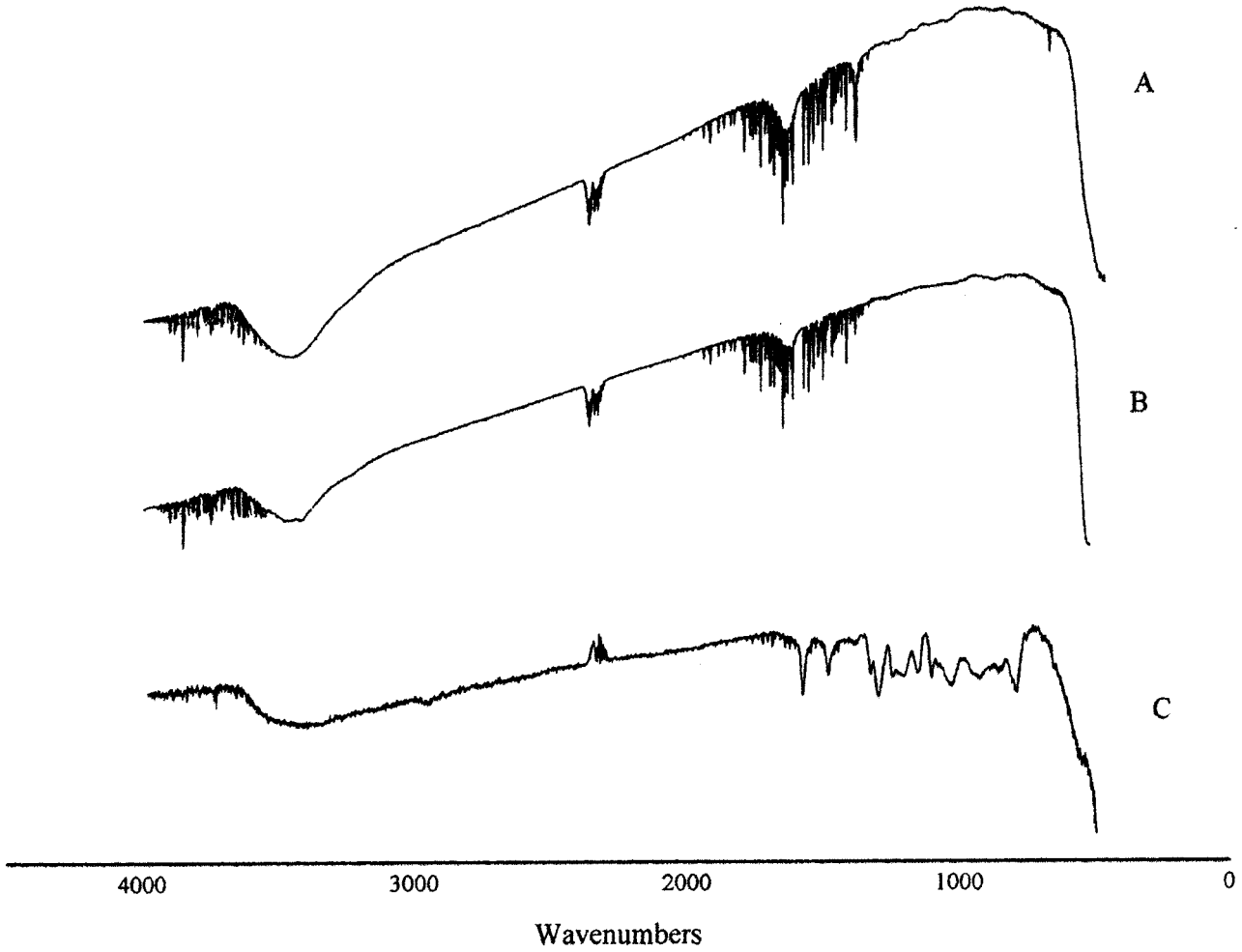


**Figure 10.** IR spectra taken after reaction with paraoxon: (A) CM−ZnO-1, (B) CM−ZnO-2, and (C) NC-ZnO.

having an average diameter of 260 nm. The small crystallite size and high surface area allows the NC−ZnO to exhibit a unique surface chemistry. This was demonstrated in reaction with a chlorocarbon, an acid gas, and an organophosphorus compound. This increase in reactivity due to particle size further supports previous work that establishes chemical reactivity as a particle size-dependent property.

**Acknowledgment.** The support of the Army Research Office is acknowledged with gratitude.

LA991498P